A Multichannel Least-Squares B-Spline Approach to Molecular Photoionization: Theory, Implementation, and Applications within the Configuration–Interaction Singles Approximation

Daniele Toffoli*,† and Piero Decleva†,‡

†Dipartimento di Scienze Chimiche e Farmaceutiche, Università degli Studi di Trieste, Via L. Giorgieri 1, I-34127, Trieste, Italy
‡CNR-IOM DEMOCRITOS, Trieste, Italy

ABSTRACT: We describe, in detail, a basis set approach to the multichannel scattering problem. The full set of linearly independent scattering states at each prefixed energy of the continuum spectrum can be obtained via a least-squares approach. To test the algorithm in a concrete setup, we report a parallel implementation of the close-coupling method in which the final states are treated within the configuration–interaction singles (CIS) approximation. The method requires, as input, a set of orthonormal orbitals, obtained from any quantum chemistry package. A one-center expansion (OCE) basis set consisting of products of radial B-splines and symmetry adapted angular functions is then used to expand the continuum electron wave function. To assess the quality of the CIS approximation, we compute total and partial cross sections and angular asymmetry parameters for the photoionization of a selection of closed-shell atoms (He, Ne, and Ar), H_2, H_2O, and ethylene. Results are compared with the experimental data and with theoretical predictions obtained with time-dependent density functional theory (TDDFT). It is seen that, generally, the photoionization observables obtained at the CIS level compare well with TDDFT predictions. The same basis can be employed to describe molecular multiphoton or strong field ionization.

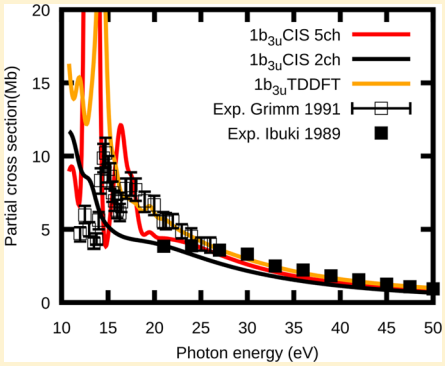

1. INTRODUCTION

The description of the photoemission process, which entails the measurement of angle-resolved photoelectron intensities, as a function of the incident photon energy, provides a wealth of information on the nature of the ground and excited states of the target sample and of the photoemission dynamics.[1] Therefore, a large class of spectroscopic techniques, such as photoelectron spectroscopy[2] (PES and XPS) and Auger electron spectroscopy[3] (AE), are also routinely used for analytical purposes, to characterize a large class of materials. Among them, resonant Auger electron spectroscopy (RAE) is currently being used to unravel the interplay of electron and nuclear dynamics following the core excitation and decay in isolated molecules, ranging from simple diatomics and triatomics to molecules of biological relevance.[4] A further interest in the detailed dynamics of the ionization process is its use as a probe of ultrafast processes in femto and attosecond pump–probe experiments (TRPES).[5]

Dominant electron correlation effects in the photoemission process can be subdivided into two main classes: *intrinsic* and *dynamic*.[6] Intrinsic correlation effects are present even in the absence of ionization, and are related to the multiconfigurational nature of bound initial and final target states; dynamic correlation effects can be described in terms of configuration–interaction (CI) in the continuum, and are usually referenced as interchannel coupling effects. An accurate description of the many-body physics of the process thus requires development of a method capable of describing, at the same level of accuracy, both bound (initial and final) states and the correlation in the continuum. This is by no means a trivial task, because standard GTO bases are of very limited use for the description of continuum states. Moreover, common quantum chemistry approaches to the many-body problem do not lend themselves naturally to the close coupling form necessary to implement continuum boundary conditions. Finally, nontrivial over-completeness problems[7] that require special treatments arise. This is the main reason most theoretical studies on small and medium size molecules are still based on a one-electron description of the phenomenon.

A renewed interest in continuum processes has arisen from spectacular advances in photon sources and multiparticle coincidence detectors. Several groups have presented different methodologies for the calculation of molecular continuum states in small polyatomics. The groups of McKoy and Lucchese have developed a general variational formalism based on the multichannel Schwinger method, together with a single center expansion of bound and continuum orbitals.[8−12] The complex Kohn approach to electron-molecule scattering and photoionization has been presented by the groups of Rescigno and McCurdy.[13−15] An approach that combines Gaussians and a discrete variable representation for the electronic continuum has been recently proposed by the same authors.[16] Moccia et al.[17,18] developed a general algorithm

based on the random-phase approximation and using large basis sets of Gaussian-type orbitals and a K-matrix-based technique. The group of Martín et al.[19,20] developed a rather sophisticated algorithm based on the use of B-splines and the solution of the time-dependent Schrödinger equation (TDSE) in a basis of vibronic states. The approach is computationally very demanding but has been applied with success to H_2^+ and H_2. Recently, they have been actively pursuing extension of the algorithms to general polyatomics.[21,22] In principle, the R-matrix approach[23,24] is capable of describing the ionization process of medium-size molecules, and it shares some common ideas with the LCAO B-spline methods that we have developed.[25−27] Recent efforts directed toward the extension of the UKRmol[28] code to compute low-energy photoionization and recombination cross sections,[29−31] has given very encouraging results. Furthermore, the full CC expansion has been recently implemented by Scrinzi et al.,[32] based on a quantum chemistry multireference configuration interaction (MRCI) description of initial and target states, plus localized correlation functions, and finite elements for the unbound electron, and the method has been applied with success to the strong-field ionization of atoms and small molecules.[32−34]

One may further mention two more restricted approaches that have received significant attention recently. One is the use of Dyson orbitals as initial states in a single-channel approach that neglects dynamic correlation, but may describe accurately intrinsic correlation in the bound states. This can be coupled either to a very simple (orthogonalized) plane of Coulomb wave for the continuum,[35] or to an accurate single-particle continuum orbital.[36] The other is the extraction of photoionization cross sections from a finite basis set pseudospectrum of bound excited states via the Stieltjes Imaging technique.[37,38] The technique allows the use of approaches developed for the treatment of bound states, and it can accurately describe both intrinsic and dynamical correlation effects;[37,38] however, lacking asymptotic boundary conditions, it cannot describe angular distributions, and cleanly separate partial cross sections, besides suffering from the relatively poor energy resolution available in practice from Stieltjes Imaging.

It is the purpose of this paper to document recent efforts to generalize algorithms developed in the group toward the implementation of a general close-coupling (CC) structure[39] of the continuum wave function, applicable in principle to general polyatomics. While the framework currently adopted for the calculation of continuum orbitals,[25−27] namely, expansion of the radial part in a B-spline basis, and the Galerkin approach and block inverse iteration for the calculation of the continuum eigenvectors remains valid,[40,41] the issue of whether a generalization of the algorithms retains their accuracy and numerical stability when the coupling of continua of different ionic states is derived from a multicentric potential still needs to be checked. Moreover, the structure and evaluation of Hamiltonian and overlap matrix elements must be completely reworked. Therefore, we present a generalization of the Galerkin approach to arbitrary closed-shell molecules where the final states are treated within the configuration−interaction singles (CIS) method[42] in a single-center basis (OCE), to take advantage of the already available algorithms for the calculations of two-electron integrals between B-splines.[40,41,43] The CIS approach has enjoyed recent popularity to describe complex physical processes driven by strong laser fields, both in atoms and molecules, as a basis for the solution of the TDSE.[44−53] In this context, the present approach is optimally suited because of its ability to fully describe the ionization continuum, and electrons reaching far out the molecular region.

The plan of the paper is as follows: in section 2, we present a summary of the CC method as applied to photoionization, while details of the multichannel generalization of the least-squares approach to the continuum spectrum, in a concrete setup provided by the CIS implementation, are presented in section 3. In section 4, we apply the formalism to the valence ionization dynamics of closed-shell atoms (He, Ne, and Ar) and polyatomics (H_2, H_2O, and ethylene). Finally, a summary and perspectives are given in section 5.

2. THEORY

The Hamiltonian of the atomic/molecular system is invariant under the operations of a given point group. The irreducible representations (irreps) of the group are labeled by a couple of indices: (λ, μ) for one-particle wave functions, and (Λ, M) for a general many-particle state. Here, λ (Λ) is the irreducible representation, and μ (M) is the degeneracy label. Moreover, since we assume the Hamiltonian to be spin independent, the total spin is also a good quantum number. To simplify the notation, we will call (ΓM) the couple of indices, which will include both space and spin symmetries, e.g., $(\Gamma M) = (\Lambda M_\Lambda S M_S)$ $\Gamma = (\Lambda, S)$; $\mathrm{M} = (M_\Lambda, M_S)$.

To exploit molecular symmetry, we work with symmetry-adapted functions, and the continuum orbitals are expanded in a symmetry-adapted angular basis, obtained from complex spherical harmonics by a unitary transformation:[54]

$$X_{j\lambda\mu} = X_{lh\lambda\mu} = \sum_m b_{mlh\lambda\mu} Y_{lm} \tag{1}$$

In eq 1, $j = lh$, where h represents the number of linearly independent angular functions $X_{lh\lambda\mu}$ for given l and symmetry λ. So $l = l(j) \equiv l_j$ and we shall use j or lh as indices interchangeably $(b_{mlh\lambda\mu} = b_{mj\lambda\mu})$. Present implementation is limited to abelian groups having real representations, namely, D_{2h} and its subgroups. A generalization to non-abelian point groups will be the focus of future works.

In photoionization, one starts with an initial bound atomic/molecular N particle state, $\Psi^N_{0\Gamma_0 M_0}$ (usually, but not necessarily, the ground state), solution of the N-particle Schrödinger equation:

$$H^N \Psi^N_{0\Gamma_0 M_0} = E^N_{0\Gamma_0} \Psi^N_{0\Gamma_0 M_0} \tag{2}$$

The target (ionic) states $\Psi_{I\Gamma_I M_I}{}^{N-1}$ will be labeled by their symmetry indices (Γ_I, M_I), which will run over all target symmetries, and an index I which counts different eigenstates within the same symmetry. They are assumed to diagonalize the $N-1$ particle Hamiltonian:

$$H^{N-1} \Psi_{I\Gamma_I M_I}{}^{N-1} = E_{I\Gamma_I}{}^{N-1} \Psi_{I\Gamma_I M_I}{}^{N-1} \tag{3}$$

Given the final total energy E in the continuum spectrum, *open channels* are all accessible target states, $(I\,\Gamma_I) = 1, ..., n_o$ (where n_o is the number of open channels), i.e., all target states with energy $E_{I\Gamma_I}{}^{N-1} < E$, corresponding to an asymptotic kinetic energy of the photoelectron $\varepsilon_{I\Gamma_I} = E - E_{I\Gamma_I} > 0$ and asymptotic momentum $k_{I\Gamma_I} = \sqrt{2\varepsilon_{I\Gamma_I}}$.

Conservation of energy can be written as

$$\varepsilon_{I\Gamma_I} = \omega - (E_{I\Gamma_I}{}^{N-1} - E_0{}^N) = \omega - \mathrm{IP}_{I\Gamma_I} \tag{4}$$

where ω is the incident photon energy, and $IP_{I\Gamma_I}$ is the ionization potential relative to the state $\Psi_{I\Gamma_I}^{N-1}$ of the ion. All other target states are called *closed channels*, where n_c is the number of closed channels and n_t is the total number of target states ($n_t = n_o + n_c$).

2.1. The Close-Coupling Wave Function. Let us consider the continuum eigenvectors of the Schrödinger equation for a given eigenvalue E, belonging to the irreps Γ_f: these solutions can be expanded in terms of basis functions, $\Phi_{\alpha\Gamma_f M_f}$, which are coupled products of the target states and the angular part of the continuum electron:

$$\Phi_{\alpha\Gamma_f M_f} = \Phi_{I\Gamma_I j\lambda\Gamma_f M_f} = \sum_{M_I\mu} \Phi_{I\Gamma_I M_I j\lambda\mu}\langle\Gamma_I M_I \lambda\mu|\Gamma_f M_f\rangle \tag{5}$$

where, in eq 5, spin coupling is implicitly included for ease of notation, and

$$\Phi_{I\Gamma_I M_I j\lambda\mu} = \Psi_{I\Gamma_I M_I}^{N-1} X_{j\lambda\mu}(\theta_N, \phi_N) \tag{6}$$

The compound index $\alpha \equiv I\Gamma_I j\lambda$ then labels the set of degenerate solutions at energy E, which are, in practical calculations, finite in number, because of the truncation of the photoelectron's angular momentum to a maximum value l_{max}.

Solutions (channel functions, $\Psi_{E\alpha'\Gamma_f M_f}^{\ N}$) can now be written in a close-coupling form:

$$\Psi_{E\alpha'\Gamma_f M_f}^{\ N} = \mathcal{A}\sum_{\alpha} \Phi_{\alpha\Gamma_f M_f} R_{E\alpha\alpha'\Gamma_f} + \sum_{K} \Phi_{K\Gamma_f M_f}^{\ N} C_{EK\alpha'\Gamma_f} \tag{7}$$

where, in eq 7, $\mathcal{A}$ is the antisymmetrizer and $R_{E\alpha\alpha'\Gamma_f}$ is the radial wave function of the continuum electron. Equivalently, dropping in the following the subspecies indices, and defining

$$\varphi_{EI\Gamma_I\lambda\alpha'\Gamma_f}(\mathbf{r}_N) = \sum_j R_{E\alpha\alpha'\Gamma_f}(r_N) X_{j\lambda\mu}(\theta_N, \phi_N) \tag{8}$$

eq 7 can be rewritten as

$$\Psi_{E\alpha'\Gamma_f}^{\ N} = \mathcal{A}\sum_{I\Gamma_I\lambda} (\Psi_{I\Gamma_I}^{\ N-1}\varphi_{EI\Gamma_I\lambda\alpha'\Gamma_f})_{\Gamma_f} + \sum_{K} \Phi_{K\Gamma_f}^{\ N} C_{EK\alpha'\Gamma_f} \tag{9}$$

In eq 9, spin coupling is included implicitly, and spatial symmetry adaptation of the N-electron wave function is symbolized as $(\cdot)_{\Gamma_f}$. According to eq 9, the solutions can be written as a sum of target states coupled to continuum wave functions plus a sum over a set of N electron localized basis functions $\Phi_{K\Gamma_f}^{\ N}$, which address the remaining square integrable part, and, in principle, can converge to the exact solutions.

Channel functions are characterized by their asymptotic behavior. It is computationally convenient to employ real "standing wave" or "K-matrix" boundary conditions, which specify the asymptotic behavior of the radial functions $R_{E\alpha\alpha'\Gamma_f}(r_N) = \frac{1}{r_N} P_{E\alpha\alpha'\Gamma_f}(r_N)$ as follows:

$$P_{E\alpha\alpha'\Gamma_f}(r) \to f_{l_j}(k_I r)\delta_{\alpha\alpha'} + g_{l_j}(k_I r) K_{\alpha\alpha'}^{\Gamma_f} \tag{10}$$

In eq 10, l_j is relative to $X_{j\lambda\mu}$, k_I is the photoelectron momentum relative to the target state $\Psi_{I\Gamma_I}^{N-1}$ ($k_I = k_{I\Gamma_I}$), and f_l, g_l are the regular and irregular radial solution of the asymptotic problem (spherical bessel functions for neutral targets o Coulomb functions in the case of charged ions). $K_{\alpha\alpha'}^{\Gamma_f}$ defines the K-matrix, real and symmetric, block diagonal on Γ_f, with dimensions equal to the number of channel functions. In actual calculations, the radial part of the photoelectron's wave function is expanded in a set of B-splines of a given order, defined in a box large enough to reach the asymptotic region. K-matrix boundary conditions are then easily implemented by fitting, in correspondence to the last two knots, the (unnormalized) radial solutions obtained from the block-inverse iteration procedure, $\bar{P}_{E\alpha\alpha'\Gamma_f}(r)$, (or, equivalently, their logarithmic derivative at the last knot) to a linear combination of the regular and irregular radial solution of the asymptotic problem:

$$\bar{P}_{E\alpha\alpha'\Gamma_f}(r) \to f_{l_j}(k_I r) A_{\alpha\alpha'} + g_{l_j}(k_I r) B_{\alpha\alpha'} \tag{11}$$

from which the K-matrix is calculated as $K^{\Gamma_f} = BA^{-1}$, and channel functions obeying K-matrix boundary conditions are obtained by the linear transformation:

$$\Psi_{E\alpha'}^{\ N} = \sum_{\beta} \bar{\Psi}_{E\beta}^{\ N} A_{\beta\alpha'}^{\ -1} \tag{12}$$

Channel functions satisfying complex, incoming-wave boundary conditions, are then obtained with a further linear transformation from the K-matrix normalized ones:

$$|\Psi_{E\alpha'}^{\ N-}\rangle = \sum_{\beta} \Psi_{E\beta}^{\ N}(1 + iK)_{\beta\alpha'}^{-1} \tag{13}$$

from which integrated cross sections and photoelectron's angular distributions are readily obtained from dipole matrix elements and phase shifts by using standard formulas.[55−57] In our implementation, the transformation from standing wave to S-matrix asymptotic conditions (eq 13) is done directly on the dipole matrix elements between the initial state and K-matrix normalized solutions.

The CC expansion (eq 7 or eq 9) generally suffers from problems of overcompleteness, even if the L^2 term on the right-hand side of eqs 7 and 9 is omitted (a "pure" CC expansion). One way to cope with this problem is to enforce orthogonality between the continuum orbitals and single-particle orbitals used to construct the bound-state wave functions. The condition then is

$$\langle\varphi_{k\lambda}|\varphi_{EI\Gamma_I\lambda\alpha'\Gamma_f}\rangle = 0 \qquad \forall\ k \tag{14}$$

However, to ensure that no single particle contributions is lost in the full CC wave function, one must ensure that all terms of the form $\Psi_{I\Gamma_I}^{\ N-1}\varphi_{k\lambda}$ are effectively contained in the space spanned by the set $\{\Phi_{K\Gamma_f}^{\ N}\}$.

3. IMPLEMENTATION OF THE CIS METHOD

We assume to have a set of occupied orthonormal atomic/molecular orbitals (AOs/MOs) $\{\varphi_{k\lambda\mu}\}$, for instance, the $N/2$ lowest energy solutions of the closed-shell restricted Hartree−Fock[58] (HF) equations for the ground-state configuration of the system, but not necessarily so. In the CIS approximation,[42] $\Psi_{0\Gamma_0}^{\ N} \equiv \Phi_0$ is the closed-shell Slater determinant built from the N spin orbitals, while target states $\Psi_{I\Gamma_I}^{\ N-1}$ are $(N-1)$-electron Slater determinants obtained from the reference state by annihilating an electron in a specific orbital. In this model, accounting for orbital relaxation following the creation of a core−hole is anticipated to be problematic if Φ_0 is the HF reference state, and it would be more convenient to start from relaxed orbitals, optimized for the ion.

Defining the OCE B-spline basis as

$$\xi_{ij\lambda\mu} = \frac{1}{r} B_i(r) X_{j\lambda\mu}(\theta, \varphi) \tag{15}$$

the N-electron basis set used to expand the channel wave functions $\Psi_{E\alpha'\Gamma_f}{}^{N}$ of eqs 7 and 9 is therefore obtained by coupling the target states $\Psi_{I\Gamma}{}^{N-1}$ with the one-particle basis $\xi_{ij\lambda\mu}$ to final symmetry $\Gamma_f M_f$. If, for the sake of simplicity, we restrict ourselves to abelian point groups, then these singlet-coupled N-electron basis functions can be written in a short-hand notation as $|^1\Phi_i^\mu\rangle$ where now the compound index $i \equiv I\,\Lambda_I$ runs on the list of the occupied spatial orbitals grouped by symmetry species, and $\mu \equiv ij$ of eq 15, since now $\lambda = \Lambda_f \otimes \Lambda_I$ and there is no need for subspecies indices, so that, henceforth, Greek letters μ ($\mu \equiv ij$) and ν ($\nu \equiv i'j'$) will be used to identify products of radial B-splines B_i ($B_{i'}$) and angular functions $X_{j\lambda}$ ($X_{j'\lambda'}$). Therefore, the task is the formulation of overlap and Hamiltonian matrix elements for the singly excited (1h−1p) singlet-coupled configurations $\Phi_i^\mu = a_\mu^\dagger a_i \Phi_0$ (spin multiplicity is henceforth omitted). A detailed derivation of the CIS equations is provided in the Appendix, so we only quote the results here. For the overlap matrix, one obtains:

$$\begin{aligned}
\langle\Phi_0|\Phi_i^\mu\rangle &= \sqrt{2}\, S_{i\mu} \\
\langle\Phi_i^\mu|\Phi_j^\nu\rangle &= \delta_{ij}\Big(S_{\mu\nu} - \sum_k S_{\mu k} S_{k\nu}\Big) + 2 S_{\mu i} S_{j\nu}
\end{aligned} \tag{16}$$

where, in eq 16, $S_{i\mu} = \langle\varphi_i|\xi_\mu\rangle$, and $S_{\mu\nu} = \langle\xi_\mu|\xi_\nu\rangle$ while the Hamiltonian matrix elements can be written as

$$\begin{aligned}
\langle\Phi_0|H|\Phi_i^\mu\rangle &= \sqrt{2}\,[E_0 S_{i\mu} + F_{i\mu} - \sum_k F_{ik} S_{k\mu}] \\
\langle\Phi_i^\mu|H|\Phi_j^\nu\rangle &= (\delta_{ij} E_0 - F_{ij})[S_{\mu\nu} - \sum_k S_{\mu k} S_{k\nu}] + \delta_{ij}[F_{\mu\nu} - \sum_l F_{\mu l} S_{l\nu} \\
&\quad - \sum_k S_{\mu k} F_{k\nu} + \sum_{kl} S_{\mu k} F_{kl} S_{l\nu}] + 2\langle\mu j|i\nu\rangle - \langle\mu j|\nu i\rangle \\
&\quad - \sum_l (2\langle\mu j|il\rangle - \langle\mu j|li\rangle) S_{l\nu} \\
&\quad - \sum_k S_{\mu k}(2\langle kj|i\nu\rangle - \langle kj|\nu i\rangle) \\
&\quad + \sum_{kl} S_{\mu k}(2\langle kj|il\rangle - \langle kj|li\rangle) S_{l\nu} \\
&\quad + 2 S_{\mu i}(F_{j\nu} - \sum_k F_{jk} S_{k\nu}) + 2 S_{j\nu}(F_{\mu i} - \sum_k F_{ki} S_{\mu k}) \\
&\quad + 2 S_{\mu i} S_{j\nu} E_0
\end{aligned} \tag{17}$$

In the derivation of eq 17, we only assumed that the reference state is a closed-shell Slater determinant constructed from a set of orthonormal orbitals. E_0 is the energy of the reference state, i.e.,

$$E_0 = \langle\Phi_0|H|\Phi_0\rangle = \sum_{i=1}^{N/2} (h_{ii} + F_{ii}) \tag{18}$$

where, in eq 18, $F = h + \sum_{i=1}^{N/2} (2J_i - K_i)$ is the Fock operator, in terms of closed-shell Coulomb and exchange operators. Then, $F_{ij} = \langle\varphi_i|F|\varphi_j\rangle$ are matrix elements of the Fock operator, between two occupied orbitals, $F_{i\mu} = \langle\varphi_i|F|\xi_\mu\rangle$ and so on. Indices k, l of eq 17 run over the set of occupied MOs in the reference state. For the two-electron matrix elements, we use the physicist's notation,[58] namely,

$$\langle\mu j|i\nu\rangle = \int\int \xi_\mu^*(\mathbf{r}_1)\varphi_j^*(\mathbf{r}_2)\frac{1}{r_{12}}\varphi_i(\mathbf{r}_1)\xi_\nu(\mathbf{r}_2)\, d\mathbf{r}_1\, d\mathbf{r}_2 \tag{19}$$

and they can be readily calculated as sums of products of MOs coefficients in the OCE basis, B-splines two electron integrals, and angular integrals.[20,41] In the special case that the MOs basis $\{\varphi_{k\lambda\mu}\}$ diagonalizes the Fock operator, i.e., $F\varphi_{k\lambda\mu} = \varepsilon_{k\lambda}\varphi_{k\lambda\mu}$, eq 17 is simplified since some terms cancel out:

$$\begin{aligned}
\langle\Phi_0|H|\Phi_i^\mu\rangle &= \sqrt{2}\,[(E_0 - \varepsilon_i) S_{i\mu} + F_{i\mu}] \\
\langle\Phi_i^\mu|H|\Phi_j^\nu\rangle &= \delta_{ij}(E_0 - \varepsilon_i)[S_{\mu\nu} - \sum_k S_{\mu k} S_{k\nu}] \\
&\quad + \delta_{ij}[F_{\mu\nu} - \sum_l \varepsilon_l S_{\mu l} S_{l\nu}] + 2 S_{\mu i} S_{j\nu} E_0 + 2\langle\mu j|i\nu\rangle \\
&\quad - \langle\mu j|\nu i\rangle - \sum_l (2\langle\mu j|il\rangle - \langle\mu j|li\rangle) S_{l\nu} \\
&\quad - \sum_k S_{\mu k}(2\langle kj|i\nu\rangle - \langle kj|\nu i\rangle) \\
&\quad + \sum_{kl} S_{\mu k}(2\langle kj|il\rangle - \langle kj|li\rangle) S_{l\nu}
\end{aligned} \tag{20}$$

but we keep the option of using non-HF orbitals of the ground state, e.g., to describe strong relaxation effects.

The core of the algorithm is the evaluation of overlap and Hamiltonian matrix elements. Operatively, the set of AOs/MOs, which represent solution of the closed-shell HF equations for the ground-state configuration of the system, are projected on the OCE basis. This procedure provides us directly with the scalar products $S_{\mu k}$ that enter in the expressions of the overlap and Hamiltonian matrix elements (see eqs 16 and 17). Instead, the $S_{\mu\nu}$ integrals are trivially obtained by radial integration. AOs have been obtained with an in-house atomic HF program in B-splines, and we checked that, to numerical accuracy, the general expression of eq 17 reduces to eq 20. For H_2, H_2O, and ethylene, restricted closed-shell MOs obtained with the MOLPRO quantum chemistry program[59] and projected on the OCE basis are no longer SCF solutions of the HF Hamiltonian in the OCE basis. Therefore, the HF Hamiltonian is rebuilt using these projected orbitals and diagonalized to get a set of $N/2$ orthonormal occupied orbitals. These orbitals are then used to evaluate the matrix elements $F_{\mu\nu}$, $F_{\mu k}$, and F_{kl} of eqs 17 and 18.

At each prefixed energy E, the correct number of linearly independent scattering states are obtained as eigenvectors relative to minimum modulus eigenvalues (actually very close to zero) of the energy-dependent matrices $A(E)$ or $A^\dagger A$, where $A(E) = H - ES$, by block inverse iteration.[25−27] The energy-independent products $H^\dagger H$, $S^\dagger S$, and $H^\dagger S + S^\dagger H$ are evaluated once and stored on disk from which $A^\dagger A$ can be assembled by linear combination at each energy. To obtain a unique solution, orthogonality constraints must be applied to the photoelectron's orbitals. In the CIS case, there is no ambiguity, and the condition reduces to require orthogonality of the continuum orbitals to those occupied in the reference state. These can be easily introduced, following the procedure outlined by Brage et al.,[7] and each orthogonality condition introduces one additional row and column to the matrix equation:

$$\begin{pmatrix} A^\dagger A(E) & b \\ b^\dagger & 0 \end{pmatrix} \begin{pmatrix} c \\ \lambda \end{pmatrix} = 0 \tag{21}$$

where, in eq 21, c is the solution vector, λ the Lagrange multiplier, and b a column vector with elements $b_\mu = \langle \varphi_i | \xi_\mu \rangle \equiv S_{i\mu}$. The number of orthogonality constraints (as checked from the inspection of the eigenvalues of the overlap matrix) corresponds to enforcing orthogonality of the continuum orbitals to all occupied orbitals of the same symmetry.

Finally, dipole matrix elements between the reference state and K-matrix normalized solutions, i.e.,

$$D_{E\alpha\gamma} = \langle \Psi^N_{E\alpha} | D_\gamma | \Phi_0 \rangle \tag{22}$$

are calculated in the molecular frame for both length and velocity form of the dipole operator. These are further transformed to S-matrix boundary conditions via the linear transformation of eq 13, from which partial cross sections and angular asymmetry parameters are calculated according to standard formulas.[55−57] The parallel implementation of the algorithm outlined above uses a standard MPI protocol[60] and proved good scaling properties up to 128 cores.

Before presenting a comparison of the accuracy of the CIS and TDDFT methods, which will be discussed at length in the forthcoming section, it is worthwhile to compare the present CIS algorithm as applied to photoionization, which is a stationary method, with other CIS methods which are based on the numerical solution of the TDSE. The core of both algorithms is the construction of the overlap and Hamiltonian matrices over the N-electron the basis of singly excited determinants (or configuration state functions). Provided that the N-electron basis spans an adequate portion of the 1h−1p space, the two methods are equivalent and give the same results in the weak-field regime, which is the focus of this paper. In our method, the dynamical observables are obtained after a generalized diagonalization of an energy-dependent matrix, while the Hamiltonian and overlap matrix calculated over the 1h−1p configurations constructed from an orthonormal spin−orbital basis ($\{\varphi_p\}$) enter into the equation of motion for the expansion coefficients of the time-dependent wave function.[32,48,49,52,53]

4. SAMPLE APPLICATIONS

To assess both the generality and robustness of the multichannel least-squares approach, and the quality of the CIS approximation to atomic/molecular photoionization, here, we report its application to a variety of atomic and molecular systems. Given this objective, we shall not discuss the systems in detail, or compare with the extensive literature available. The noble gases helium, neon, and argon have been the subject of a large amount of experimental investigations and theoretical predictions. H_2 and H_2O are among the best studied molecular systems. The valence photoionization of ethylene has been the subject of several theoretical and experimental studies.[61−66] However, the theoretical methods employed were restricted to single-channel approaches,[61,66] and therefore it is worthwhile to investigate how interchannel coupling affects the photoionization dynamics of the outermost ionizations. Since both CIS and TDDFT are relatively simple computational schemes that can be applied to large molecules, it is also important to judge the CIS performances, with respect to the more widely used TDDFT. For CIS, transition-matrix elements are calculated in both the length and velocity forms of the dipole operator. Cross sections and angular asymmetry parameters calculated in both gauges will be presented and compared with the available experimental data and results of TDDFT calculations that employ the LB94[67] xc functional and that use the same OCE B-spline basis set. Otherwise explicitly stated, all dipole allowed channels are included in CIS and TDDFT calculations.

In all calculations, B-splines of order 10 have been employed, and a linear grid of knots with step size of h = 0.2 a.u. The range of the grid (R_{max}) is 10. a.u. for helium, and 20 a.u. for all other systems (h = 0.25 a.u. and R_{max} = 25 a.u. for H_2). For all molecules, the ground-state HF orbitals were obtained with an aug-cc-pVTZ basis set and the MOLPRO[59] program, and then projected onto the OCE B-spline basis. All results reported are convergent with respect to the basis, namely the radial grid step, the range of the radial grid and the number of asymptotic angular momenta included, as checked by preliminary calculations at the CIS and TDDFT level.

4.1. Valence Photoionization of Helium, Neon, and Argon. The CIS total cross sections in both the length (denoted hereafter as CIS-len) and velocity (denoted hereafter as CIS-vel) form of the dipole operator for helium are reported in Figure 1, along with the available experimental data,[68,69] a

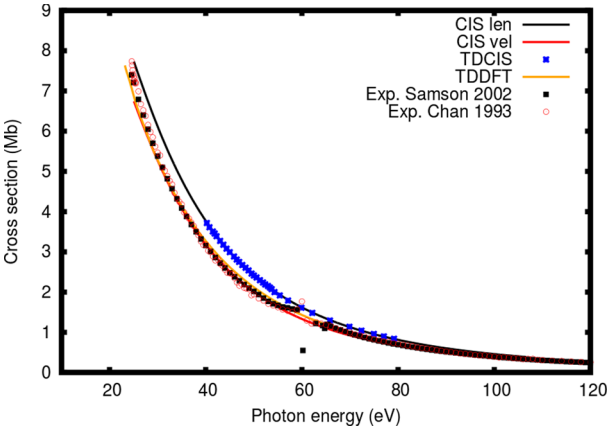

Figure 1. CIS photoionization cross section of He in both length and velocity forms of the dipole operator, and comparison with the available experimental data,[68,69] recent TD-CIS results,[51] and a TDDFT calculation (this work).

recent time-dependent CIS (TD-CIS) calculation,[51] and the TDDFT results. The TD-CIS formalism is based on the direct solution of the time-dependent Schrödinger equation, while our method is based on a time-independent formulation of scattering theory. The two methods give exactly the same results (the TD-CIS results were obtained in the length gauge[51]). This furnished a good indication of the correctness of our implementation. The comparison between the CIS results and the experimental data indicates generally good agreement, especially at higher photoelectron kinetic energy. In particular, while the CIS-len cross section slightly overestimates the total intensity, the CIS-vel results agree perfectly with both TDDFT predictions and the experimental data. The dip in the experimental total cross section at ∼60 eV of photon energy is the signature of two-electron excited states, which are not included in either CIS or TDDFT formalisms. Since He has only the 1s orbital occupied, from symmetry considerations, the angular asymmetry parameter has a constant, energy-independent value of 2, and is therefore not reported.

The electronic configuration of Ne is $1s^2 2s^2 2p^6$. The CIS total cross sections of Ne are reported in Figure 2, up to a photon energy of ∼120 eV, along with the experimental values

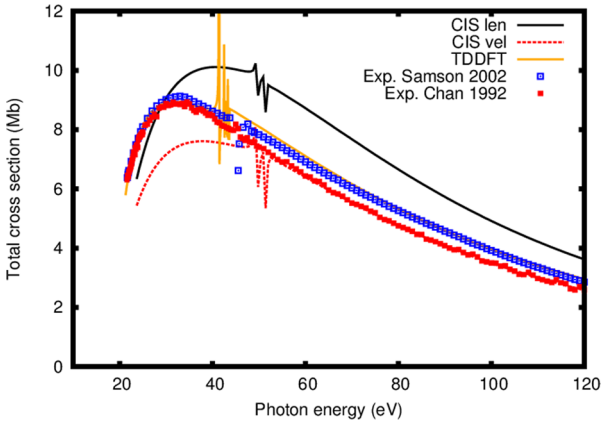

Figure 2. Total photoionization cross section of Ne. CIS results in both length and velocity forms are reported along with the available experimental data[70,71] and the TDDFT results.

from the literature[70,71] and the TDDFT results. The two sets of experimental data agree in the near threshold region up to ~44 eV of photon energy. Above 44 eV, the more recent experimental data of Samson et al.[71] lie consistently above the dipole (e,e) results of Chan et al.[70] Overall, the TDDFT results agree better with both experimental datasets when compared to the CIS predictions, expecially in the near-threshold region. The CIS-len results overestimate the experimental data while the CIS-vel profile underestimates them. Above 44 eV, the CIS-vel results agree perfectly with the older experimental data,[70] while the TDDFT predictions are consistent with the more-recent photoionization cross-section measurements.[71] Since a TDDFT treatment of the photoionization dynamics does include interchannel coupling only among singly excited configurations, as the CIS method, a disagreement between the two treatments must, at least in part, be due to the different treatment of correlation effects in the bound states (both the ground state and the ionized target states). Another possible reason is that TDDFT can, at least in an average way, describe double excitations, which are completely absent in the CIS approximation. On the other hand, we should also keep in mind that the close-coupling implementation is, in principle, general, and correlation in the initial and final ionic states can be introduced later in a systematic way within *ab initio* CC approaches, at variance with DFT.

The asymmetry parameter profile for the 2p orbital ionization of Ne is reported in the upper panel of Figure 3. The asymmetry parameter starts from negative values at the threshold and is then characterized by a monotonic increase up to a value close to 1.5 for higher excitation energies. The modulations in the CIS profiles at ~45 eV, which are more visible in the total cross section profiles, are due to singly excited configurations decaying in the continuum (autoionization resonances). Overall, there is good agreement between the theoretical CIS and TDDFT profiles and the experimental data.[72] The $2s^{-1}$ partial cross section of Ne is reported in the lower panel of Figure 3. Here, we see that both CIS cross sections are in much better agreement with the experiment,[73] compared to the TDDFT results, which, in turn, overestimates the cross section by a factor of ~3. This large discrepancy between TDDFT and the experimental data is attributed to the incorrect treatment of exchange in TDDFT.[74]

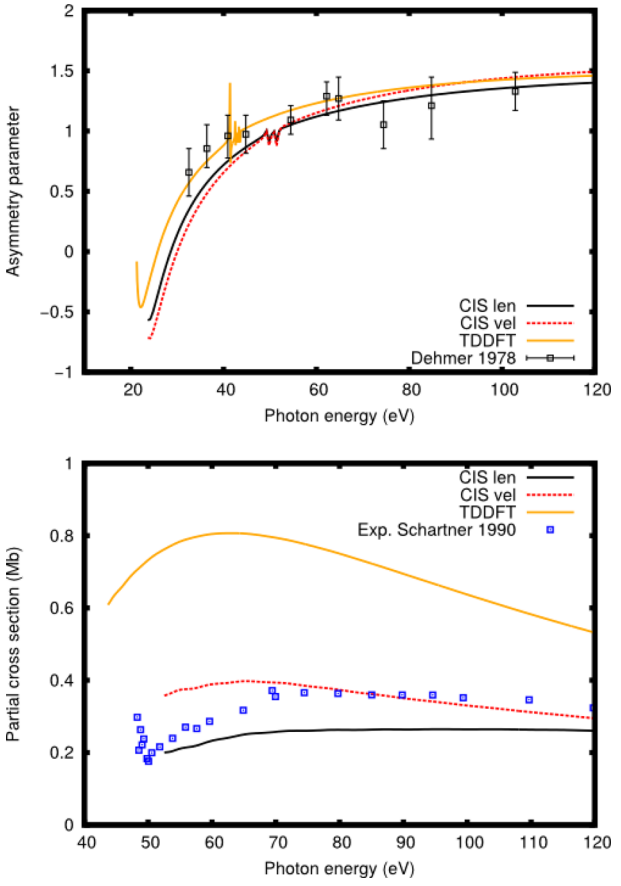

Figure 3. (Upper panel) CIS asymmetry parameter profiles for the $2p^{-1}$ ionization of Ne, and comparison with experimental data[72] and TDDFT results. (Lower panel) CIS Ne partial 2 s^{-1} photoionization cross sections and comparison with the experimental data[73] and TDDFT results.

The electronic configuration of Ar is $[Ne]3s^23p^6$. The total cross section of Ar is reported in Figure 4, up to a photon energy of ~120 eV, along with the experimental values from the literature.[71,75] The CIS profiles are in qualitative agreement with experimental data from various sources:[71,75] both predict the occurrence of a delayed onset of the $3p \rightarrow \epsilon d$ channel, with a maximum at a photon energy of ~25 eV and the occurrence of a Cooper's minimum at higher photon energies. However, disagreement does exist concerning both the absolute value of cross section at the maximum, and the exact energy position of the Cooper's minimum (lower panel of Figure 4). The Cooper's minimum is a one-electron effect, since it is related to the presence of a radial node in the 3p orbital of Ar; consequently, the dipole matrix element for the transition $3p \rightarrow \epsilon d$ changes sign as the photoelectron kinetic energy increases.

In Figure 5, we report the $3p^{-1}$ asymmetry parameter profile (upper panel) and the $3s^{-1}$ partial cross section (lower panel). The occurrence of the Cooper's minimum in the $3p^{-1}$ ionization channel is responsible for the strong modulation of the 3p angular asymmetry parameter, visible in Figure 5. Both CIS and TDDFT calculations agree well with the experimental data[76] available. The agreement between experimental data and the calculations is fair in the case of the $3s^{-1}$ partial cross section. Interchannel coupling effects between the $3s^{-1}$ and $3p^{-1}$ are responsible for the occurrence of a cross-sectional minimum in the 3s ionization cross section. We note that, in the CIS calculations, the position of the minimum is strongly

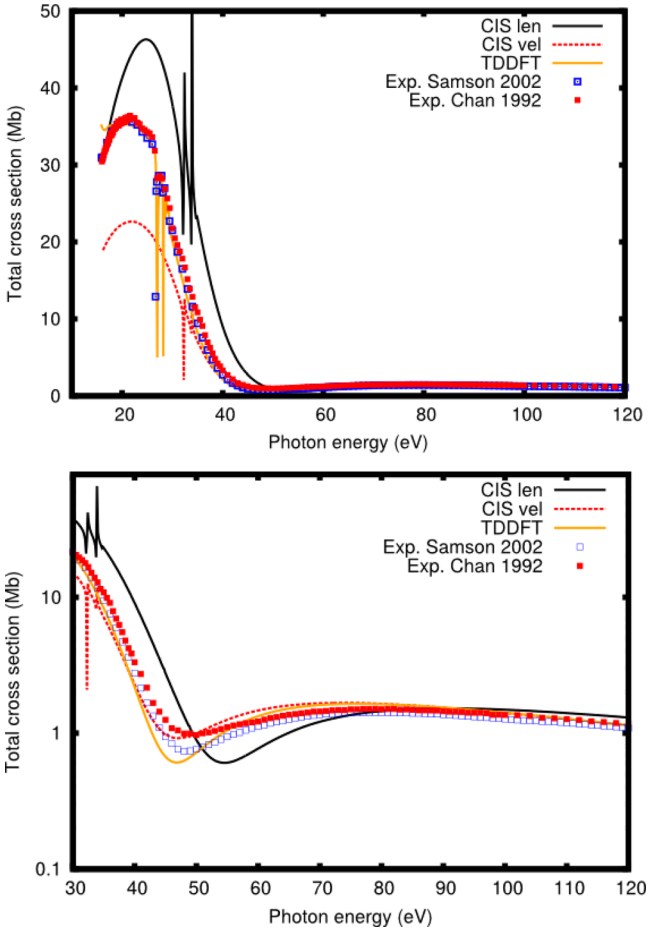

Figure 4. CIS and TDDFT total photoionization cross section profiles for Ar, and comparison with the available experimental data.[71,75] The Cooper's minimum in the total cross section is clearly visible in the lower panel at ~50 eV.

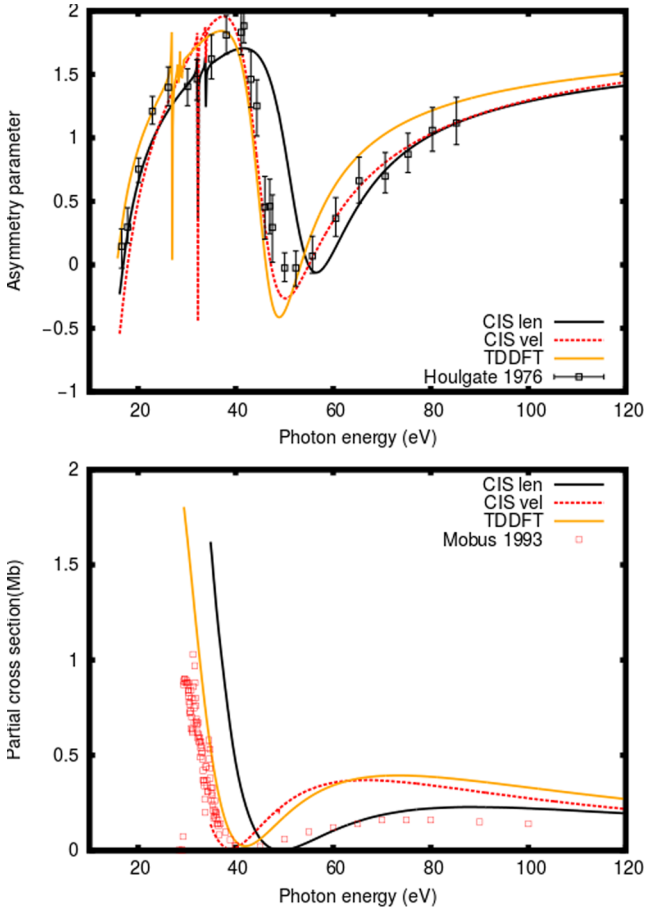

Figure 5. (Upper panel) CIS and TDDFT asymmetry parameter profiles for the 3p ionization of Ar, and comparison with the available experimental data.[76] (Lower panel) CIS and TDDFT partial 3 s^{-1} photoionization cross sections and comparison with experimental data.[77]

dependent on the dipole gauge, and again the CIS results in the velocity form of the dipole operator is in somewhat better agreement with the experimental data.[77] At higher energy, instead, the length form seems to reproduce the experimental results somewhat better.

4.2. Valence Photoionization of H_2, H_2O, and Ethylene. H_2 provides a good test of the methodology, since the nonspherical molecular potential couples different angular momentum channels and, thus, also increases the computational complexity. Since there is only one ionized state ($1\sigma_g^{-1}$), interchannel coupling effects between main-line channels are absent. However, the importance of two-electron excited configurations can be assessed by comparison of the CIS and TDDFT predictions with the experimental data. The origin of the single-center expansion has been put in the center of mass of the system. The maximum value of angular momentum used in the partial wave expansion of the continuum orbitals is l_{max} = 10. In preliminary calculations, we checked that this parameter is sufficient to obtain very convergent results for both the cross section and the angular asymmetry parameter.

In Figure 6, we report the photoionization cross section and the angular asymmetry parameter for the ionization of the $1\sigma_g$ orbital, and a comparison with the available experimental data.[78,79] Concerning the total cross section, TDDFT and CIS results in the velocity gauge are both in excellent agreement with the experimental data of Samson et al.,[78] while CIS results obtained in the length gauge slightly overestimate the experimental data. For both the cross section and the angular asymmetry parameter, the CIS results (velocity form) are also in excellent agreement with recent static-exchange calculations of Zimmermann et al.[79] The agreement of the theoretical data with the most recent experimental values[79] of the asymmetry parameter is fair in the entire spectral region investigated. Low-energy scatter in the experimental β values at a photon energy of ~30 eV are attributed to the occurrence of doubly excited states,[80] which are not included in our CIS and TDDFT calculations.

We present the total photoionization cross section of H_2O in Figure 7. In water, beside the coupling of different continuum partial waves, due to the nonspherical nature of the potential, we also have interchannel coupling effects between main-lines. The origin of the single-center expansion has been put on the O atom. The maximum value of angular momentum used in the partial wave expansion of the continuum orbitals is l_{max} = 6, which provides convergent results for both cross sections and angular asymmetry parameters in the entire photon energy range explored. Strong near-threshold modulations in both CIS and TDDFT profiles are due to autoionization resonances that have been smoothed by convolution of the calculated profiles with Gaussian functions having a full-width at half-maximum (fwhm) of 1.0 eV.

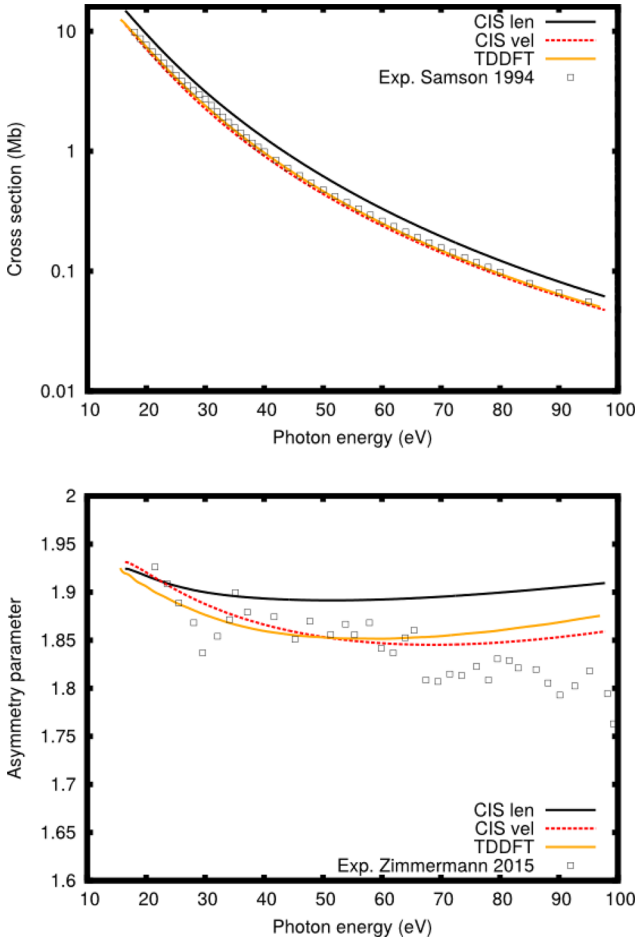

Figure 6. CIS and TDDFT photoionization cross sections (upper panel) and asymmetry parameter profiles (lower panel) for the $1\sigma_g^{-1}$ ionization of H_2.The available experimental data from the literature[78,79] have also been reported.

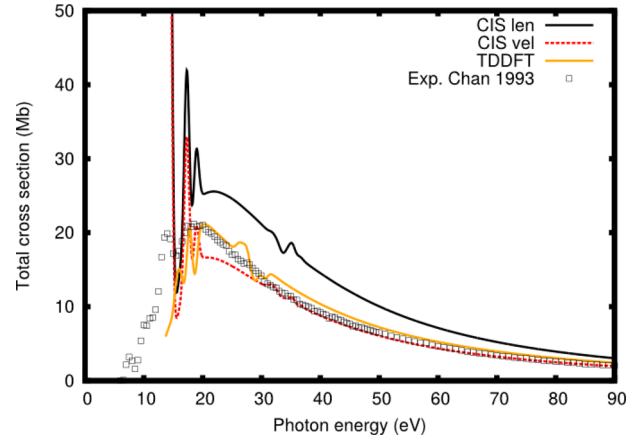

Figure 7. CIS and TDDFT total photoionization cross sections of H_2O and comparison with experimental data.[81]

The predicted sharp autoionization features are not visible in the experimental data, partially due to the experimental resolution, and partially due to our neglect of vibrational effects that broaden the spectral features. As noted in several instances in this work, while there is nice agreement between TDDFT, CIS results in the velocity gauge, and the experimental data over the entire energy region, the CIS results in the length gauge have a tendency to overestimate the total cross section, although all three theoretical curves present a similar shape.

This trend is also apparent from the inspection of the partial cross sections for the $1b_1^{-1}$, $1b_2^{-1}$, and $3a_1^{-1}$ ionic states, which are reported in Figure 8, along with the corresponding asymmetry parameter profiles. With the exception of the partial cross section for the production of the $1b_2^{-1}$ ionic state, CIS results in the velocity form and TDDFT are of comparable accuracy, while CIS results in the length gauge invariably overestimate the experimental cross sections.[82,83] A close agreement between CIS-len and CIS-vel results is obtained for the asymmetry parameters profiles, where the agreement with the experimental data[82,84] can be considered quantitative.

The electronic configuration of the ground state of ethylene (D_{2h} symmetry) is

$$KK(2a_g)^2(2b_{1u})^2(1b_{2u})^2(3a_g)^2(1b_{3g})^2(1b_{3u})^2(^1\Sigma_g^+)$$

The origin of the single-center expansion has been put on the middle of the C=C double bond. The maximum value of angular momentum used in the partial wave expansion of the continuum orbitals is given as l_{max} = 18, which provides convergent results for both cross sections and angular asymmetry parameters for the $1b_{3u}^{-1}$ and the $1b_{3g}^{-1}$ ionizations in the entire photon energy range explored. To assess the effects of interchannel coupling on the computed observables, we carried out two sets of calculations: a two-channel calculation (CIS-2ch), where only coupling between the continuum partial waves from the $1b_{3u}^{-1}$ and the $1b_{3g}^{-1}$ target states were included, and a five-channel calculation (CIS-5ch), where all dipole-allowed channels originating from the outermost five ionizations were included in the close-coupling expansion. Since photoionization observables calculated in the velocity gauge of the dipole operator are generally in better agreement with the experimental data, compared to the results obtained in the length gauge, and to avoid cluttering of the figures, we have decided not to display the latter. Suffice to say that, as observed for the other systems presented in the paper, partial cross sections obtained in the length gauge are invariably overestimated, compared to both CIS (velocity gauge) and TDDFT profiles, while, generally, a much closer agreement between the two gauges is obtained for the asymmetry parameter profiles. Strong near-threshold modulations in both CIS and TDDFT profiles, which are due to autoionization resonances not resolved in the experimental data, have been smoothed by convolution of the calculated profiles with Gaussian functions of full-width at half-maximum of 1.0 eV.

The cross section and asymmetry parameter profiles for the ionization leading to the ground ionic state, X^2B_{3u}, and the A^2B_{3g} of ethylene are reported in Figure 9. We start our discussion with the ionization from the HOMO ($1b_{3u}^{-1}$), which is of π character. The near-threshold photoionization dynamics is dominated by resonant features due to autoionization, which can be described both at the CIS and TDDFT levels, but not at the single-channel level. In fact, both frozen-core HF (FCHF) and continuum multiple scattering (CMS) calculations are not able to predict the strong oscillatory behavior of the experimental data in this energy range but show a smooth decreasing behavior.[61,66] In the near-threshold energy range, the CIS-5ch profile is in somewhat better agreement with both TDDFT and the experimental data, compared to the CIS-2ch profile. However, there are some discrepancies between

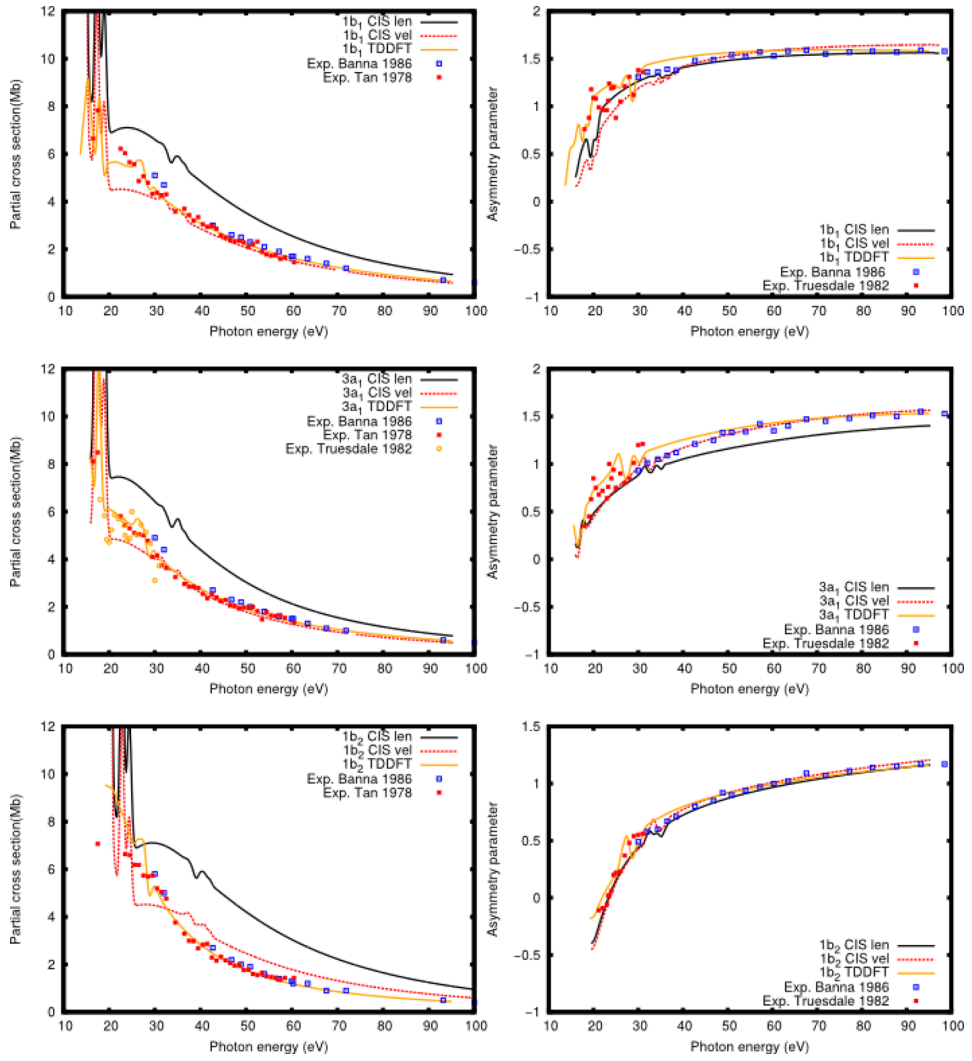

Figure 8. (Left) CIS and TDDFT partial photoionization cross sections for the $1b_1^{-1}$ (upper panel), $3a_1^{-1}$ (central panel), and $1b_2^{-1}$ (lower panel) ionizations of H_2O and comparison with the experimental data.[82,83] (Right) CIS and TDDFT asymmetry parameter profiles for the $1b_1^{-1}$ (upper panel), $3a_1^{-1}$ (central panel), and $1b_2^{-1}$ (lower panel) ionizations of H_2O and comparison with the experimental data.[82,84]

theoretical (CIS-5ch and TDDFT) profiles and the experimental data that demand further experimental verification. Compared to the CIS-5ch calculation, the TDDFT result shows sligthly better agreement with the experiment in the photon energy interval of 15−25 eV, whereas, for higher excitation energies, all theoretical profiles rapidly converge to the experimental points. Concerning the asymmetry parameter profile, we see that neither the two CIS calculations nor TDDFT can achieve a quantitative agreement with the experiment in the energy region of autoionizating states. Above a photon energy of 20 eV, the agreement between theoretical profiles (CIS-5ch, TDDFT) and the experiment can be considered quantitative, at variance with earlier FCHF and CMS results.[61,66] The near-threshold dynamics of the $1b_{3g}^{-1}$ ionization carries signatures of both one-electron and multielectron resonances. Earlier CMS and FCHF calculations predicted, in agreement with our CIS-2ch results (not shown in the figure), the occurrence of shape resonances in the kb_{1u} and kb_{2u} channels, and are in surprisingly good agreement with the available experimental data for both cross section and asymmetry parameter profiles.[61,66] In addition to this resonant behavior, both CIS-5ch and TDDFT calculations predict the occurrence of autoionizating decay of excited states, giving rise to strong modulations that have been partially washed out by the convolution procedure. It is interesting to note (i) the good agreement between TDDFT and CIS-5ch profiles for both partial cross section and asymmetry parameter and (ii) the CIS-2ch calculation gives results in better agreement with the experimental data, which is surprising, and probably fortuitous, but consistent with the good agreement between the experimental data and predictions from single-channel theories, as observed in the literature.[61,66] For higher excitation energies, the calculated cross-sectional profiles rapidly converge to the experimental data available, while the CIS-5ch and TDDFT asymmetry parameter profiles are observed to underestimate the experimental data.

5. CONCLUSIONS AND OUTLOOK

In this paper, we present a multichannel continuum algorithm at the *ab initio* configuration−interaction singles (CIS) level,[42] based on a B-spline basis, Galerkin approach, and block inverse iteration for the calculation of the continuum eigenvectors. The core of the algorithm is the calculation of Hamiltonian and overlap matrix elements in a multielectron basis of close-

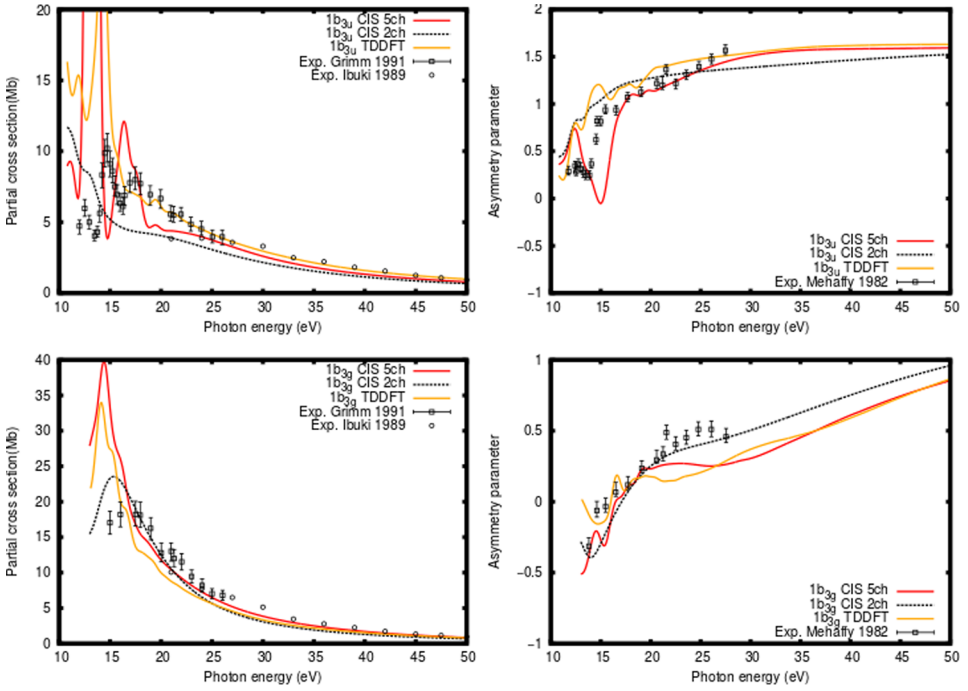

Figure 9. (Left) Five-channel CIS, two-channel CIS, and TDDFT partial photoionization cross sections for the $1b_{3u}^{-1}$ (upper panel), and $1b_{3g}^{-1}$ (lower panel) ionizations of ethylene and comparison with the experimental data.[62,65] (Right) Five-channel CIS, two-channel CIS, and TDDFT asymmetry parameter profiles for the $1b_{3u}^{-1}$ (upper panel), and $1b_{3g}^{-1}$ (lower panel) ionizations of ethylene, and comparison with the experimental data.[64]

coupling form, as antisymmetrized products of target (ionic) state eigenfunctions times a B-spline function to describe the continuum electron. As such, it is immediately generalizable to correlated target states. Moreover, such a basis is ideally suited to describe multiphoton or strong field ionization phenomena via solution of the TDSE, without the limitations of the usual GTO bases,[44−46] and allows extraction of the fully energy and angle-resolved cross sections. Actually, the more elaborate B-spline ADC(2) approach has been already employed in the calculation of total cross section via Stieltjes Imaging, or high harmonic generation.[85] However, because of the lack of proper boundary conditions, it is not currently possible to employ that approach for full continuum calculations.

To test the new algorithms in a concrete setup, we presented a generalization of the Galerkin approach to arbitrary closed-shell molecules, where the final states are treated within the configuration interaction singles method.[42] The continuum wave function is expanded in a single-center basis, taken as a product of symmetry-adapted angular functions and radial B-splines functions, to take advantage of the already available algorithms for the calculations of two-electron integrals between B-splines.[40,41] This represents the first step toward the implementation of a general close-coupling (CC) structure[39] applicable to general polyatomics. Details of the implementation are presented, in particular, the structure and evaluation of Hamiltonian and overlap matrix elements. Since the CIS method has been only sparsely applied to the study of atomic/molecular photoionization dynamics, here, we present several applications to the valence ionization dynamics of closed-shell atoms (He, Ne, Ar) and polyatomics (H_2, H_2O, and ethylene). Partial cross sections and asymmetry parameter profiles for atoms and randomly oriented molecules have been calculated in both length and velocity form of the dipole operator, and compared with TDDFT and the experimental data, when available. In almost all instances, CIS results in the velocity gauge are in very good agreement with the experimental data and with TDDFT predictions. The Ne 2s ionization is well-described at the CIS level, whereas, because of the incorrect treatment of exchange, it represents a pathological case for TDDFT. Since both CIS and TDDFT are relatively simple and inexpensive methods for the calculation of molecular excited states, we anticipate that CIS could be used as an alternative to TDDFT for all cases where TDDFT loses its predictive power, because of inaccuracies in existing exchange-correlation functionals (e.g., charge transfer excitations,[74] which are commonly observed in transition-metal compounds).

To boost the applicability of the CIS method to medium-sized molecules, one must supplement the OCE expansion with basis sets centered on the off-center atoms.[25,27,86] This requires new algorithms for the calculation of the two-electron integrals between basis functions located on different centers. A parallel algorithm based on the solution of the Poisson's equation is being currently developed in the group, and tests of its accuracy are underway.

Although CIS and TDDFT are among a restricted number of computational methods beyond mean-field approaches that can be used for the calculation of the excitation spectrum and ionization dynamics of large molecular systems, the restriction of the excitation space to the 1h−1p manifold usually cannot provide an accurate description of the residual electron−electron interaction,[87] although this impacts different observables in different ways. In fact, the impact of multielectron excitations in computed vertical excitation energies is reflected in large absolute errors for the excitation spectrum of water computed at the CIS level, compared to other *ab initio* methods, specifically multireference methods, that include a larger portion electron correlation effects,[87] but it is somewhat less pronounced in the case of computed asymmetry parameter profiles, as evidenced from the results reported in this work.

In atomic and molecular single photon ionization, accounting for both static and dynamic electron correlation effects is needed for an accurate description of the dynamics of the process.[7,10,37,88,89] In fact, the lack of correlation in the target states (as, for example, when using approximate HF target states) can sometimes overestimate the extent of continuum correlation effects (interchannel coupling).[90] Multielectron excitations have also been recently demonstrated to affect multiphoton and strong-field ionization.[32,34,51,91] An accurate treatment of the ionization process thus requires a balanced description of both static and dynamic correlation effects. The former can be included by allowing a multiconfigurational description of N electron initial and ionized target states, which can be achieved by using standard quantum-chemistry approaches, such as multiconfigurational self-consistent field (MCSCF), restricted configuration−interaction (CI) expansions,[10,29,88] or multireference CI methods,[32] while the latter is automatically included in the form of a close coupling approach (as described in this paper) with carefully chosen ionic states and penetration terms that are needed for the description of final-state correlation effects.[12,92,93]

In conclusion, the multichannel algorithm described in this work is efficient, stable, and general, and it requires relatively small modifications for the use of correlated wave functions for the bound states involved. These currently can be obtained from standard quantum chemistry approaches, such as complete-active-space self-consistent field (CASSCF) methods and multireference CI, in a Gaussian basis. This task requires the extraction of reduced density matrices up to three particles, which will be the subject of future works.

APPENDIX: REDUCTION OF MANY-PARTICLE MATRIX ELEMENTS

Here, we give a complete derivation of eqs 16 and 17 in the paper. We assume to have n orthonormal orbitals $\{\varphi_i\}_{i=1,...,n}$, which define the reference configuration $\Phi_0 = |\varphi_1, ..., \varphi_n\rangle$. These can be considered members of a complete orthonormal set $\{\varphi_p\}_{p=1,...,\infty}$. We shall adopt the following convention for the indices: $i, j, k, l, ...$ for the orbitals occupied in the reference configuration, $a, b, ...$ for the orbitals not occupied in the reference ket, while $p, q, ...$ will denote generic elements of the basis, so that $\sum_p = \sum_i + \sum_a$. The derivation proceeds in two steps. We will first derive expressions for the CIS Hamiltonian and overlap matrix elements for singlet spin eigenfunctions (or configuration state functions, CSFs) associated with the case of a closed-shell restricted reference determinant, Φ_0. The case of single excitations into a separate nonorthogonal basis, which leads to eqs 16 and 17 in this paper, will then be described in detail.

A.1. Singlet Configuration State Functions (CSFs) from a Closed-Shell Determinant

Consider the set of 1h1p states as single determinants in the orthonormal spin-orbital basis $\{\varphi_p\}$, defined with respect to Φ_0 (that is, $\{\Phi_i^p\} = \{\Phi_i^a\} + \{\Phi_i^k\}$. Only Φ_i^a are true excited states; however, it will be useful to consider also determinants $\Phi_i^k = \delta_{ik}\Phi_0$. Since the spin-orbital basis is orthonormal, the following relations are straightforwardly obtained:

$$\langle \Phi_i^a | \Phi_j^b \rangle = \delta_{ij}\delta_{ab}$$
$$\langle \Phi_i^k | \Phi_j^b \rangle = 0$$
$$\langle \Phi_i^k | \Phi_j^l \rangle = \delta_{ik}\delta_{jl} \tag{A1}$$

while the Fock operator, with respect to Φ_0, reads

$$F = h + \sum_j \langle \varphi_j || \varphi_j \rangle \tag{A2}$$

with matrix elements $F_{pq} = h_{pq} + \sum_j \langle pj||qj\rangle$.

By using standard Slater−Condon rules[58] for the matrix elements of one- and two-electron operators between N-electron Slater determinants, we obtain the following expressions for the Hamiltonian matrix elements over singly excited determinants:

$$\langle \Phi_0 | H | \Phi_0 \rangle = E_0 = \sum_i h_{ii} + \sum_{i<j} \langle ij||ij\rangle = \frac{1}{2}\sum_i (h_{ii} + F_{ii})$$
$$\langle \Phi_0 | H | \Phi_i^a \rangle = F_{ia}$$
$$\langle \Phi_i^a | H | \Phi_j^b \rangle = \delta_{ij}\delta_{ab}E_0 + \delta_{ij}F_{ab} - \delta_{ab}F_{ij} - \langle aj||bi\rangle$$
$$\langle \Phi_i^k | H | \Phi_j^b \rangle = \delta_{ik}F_{jb}$$
$$\langle \Phi_i^k | H | \Phi_j^l \rangle = \delta_{ik}\delta_{jl}E_0 \tag{A3}$$

Since we are only interested in singlet coupled configurations defined as

$${}^1\Phi_i^a = \frac{1}{\sqrt{2}}(\Phi_i^a + \Phi_{\bar{i}}^{\bar{a}}) \tag{A4}$$

(here, an overbar is used to denote β spin), by using eqs A1 and A3, we obtain the following for the overlap and Hamiltonian matrix elements, respectively (all indices now refer to spatial orbitals):

$$\langle {}^1\Phi_i^a | {}^1\Phi_j^b \rangle = \delta_{ij}\delta_{ab}$$
$$\langle {}^1\Phi_i^k | {}^1\Phi_j^b \rangle = 0$$
$$\langle {}^1\Phi_i^k | {}^1\Phi_j^l \rangle = 2\delta_{ik}\delta_{jl} \tag{A5}$$

and

$$\langle {}^1\Phi_i^a | H | {}^1\Phi_j^b \rangle = \delta_{ij}\delta_{ab}E_0 + \delta_{ij}F_{ab} - \delta_{ab}F_{ij} + 2\langle aj|ib\rangle - \langle aj|bi\rangle$$
$$\langle {}^1\Phi_i^k | H | {}^1\Phi_j^b \rangle = 2\delta_{ik}F_{jb}$$
$$\langle {}^1\Phi_i^k | H | {}^1\Phi_j^l \rangle = 2\delta_{ik}\delta_{jl}E_0 \tag{A6}$$

A.2. Single Excitations into a Separate Nonorthogonal Basis

To derive eqs 16 and 17, we need to consider a second, nonorthogonal, one-electron basis, i.e., the OCE B-spline basis of eq 15, $\{\xi_\mu\}$. Call the overlap matrix elements $\langle \xi_\mu | \xi_\nu \rangle = S_{\mu\nu}$ and $\langle \varphi_i | \xi_\mu \rangle = S_{i\mu}$. We can develop the generic basis element ξ_μ into the complete orthonormal basis ϕ_p as follows:

$$\xi_\mu = \sum_p \varphi_p \langle \varphi_p | \xi_\mu \rangle = \sum_p \varphi_p S_{p\mu} = \sum_a \varphi_a S_{a\mu} + \sum_k \varphi_k S_{k\mu} \tag{A7}$$

In the following, we consider only singlet-spin configurations and omit the spin multiplicity index. By using eq A7, the overlap matrix element $\langle\Phi_i^\mu|\Phi_j^\nu\rangle$ of eq 16 can be written as

$$\langle\Phi_i^\mu|\Phi_j^\nu\rangle = \sum_{pq} S^*_{p\mu}S_{q\nu}\langle\Phi_i^p|\Phi_j^q\rangle = \sum_{ab} S^*_{a\mu}S_{b\nu}\delta_{ij}\delta_{ab} + \sum_{kl} S^*_{k\mu}S_{l\nu}2\delta_{ik}\delta_{jl}$$
$$= \delta_{ij}\sum_a S_{\mu a}S_{a\nu} + 2S_{\mu i}S_{j\nu} \tag{A8}$$

where, in deriving eq A8, the results of eq A5 have been used. To obtain the result quoted in eq 16, we note that the sum over the full set of virtual orbitals φ_a, appearing on the right-hand side of eq A8, can eventually be replaced by a sum over the orbitals occupied in the reference ket $|\Phi_0\rangle$ by using the property of completeness of the orthonormal basis $\{\varphi_p\}$. Along the same lines, one obtains the expression for $\langle\Phi_0|\Phi_i^\mu\rangle$ quoted in eq 16. The expressions for the Hamiltonian matrix elements reported in eq 17 are derived along similar lines. By using eq A7, the matrix element $\langle\Phi_i^\mu|H|\Phi_j^\nu\rangle$ can be written as

$$\langle\Phi_i^\mu|H|\Phi_j^\nu\rangle = \sum_{pq} S^*_{p\mu}S_{q\nu}\langle\Phi_i^p|H|\Phi_j^q\rangle$$
$$= \sum_{ab} S_{\mu a}S_{b\nu}\langle\Phi_i^a|H|\Phi_j^b\rangle + \sum_b S_{\mu i}S_{b\nu}\langle\Phi_i^i|H|\Phi_j^b\rangle$$
$$+ \sum_a S_{\mu a}S_{j\nu}\langle\Phi_i^a|H|\Phi_j^j\rangle + S_{\mu i}S_{j\nu}\langle\Phi_i^i|H|\Phi_j^j\rangle \tag{A9}$$

Let us consider each term appearing on the right hand side of eq A9 separately. For the first term, by using the results of eq A6, together with the completeness of the $\{\varphi_p\}$ basis, one obtains

$$\sum_{ab} S_{\mu a}S_{b\nu}\langle\Phi_i^a|H|\Phi_j^b\rangle = (\delta_{ij}E_0 - F_{ij})[S_{\mu\nu} - \sum_k S_{\mu k}S_{k\nu}]$$
$$+ \delta_{ij}[F_{\mu\nu} - \sum_l F_{\mu l}S_{l\nu} - \sum_k S_{\mu k}F_{k\nu} + \sum_{kl} S_{\mu k}F_{kl}S_{l\nu}] + 2\langle\mu j|i\nu\rangle$$
$$- \langle\mu j|\nu i\rangle - \sum_l (2\langle\mu j|il\rangle - \langle\mu j|li\rangle)S_{l\nu}$$
$$- \sum_k S_{\mu k}(2\langle kj|i\nu\rangle - \langle kj|\nu i\rangle) + \sum_{kl} S_{\mu k}(2\langle kj|il\rangle - \langle kj|li\rangle)S_{l\nu} \tag{A10}$$

For the second term, one obtains

$$\sum_b S_{\mu i}S_{b\nu}\langle\Phi_i^i|H|\Phi_j^b\rangle = \sqrt{2}\,S_{\mu i}\sum_b S_{b\nu}\sqrt{2}\,F_{jb}$$
$$= 2S_{\mu i}(F_{j\nu} - \sum_k F_{jk}S_{k\nu}) \tag{A11}$$

Similarly, the third and the last term can be reduced to the following expressions:

$$\sum_a S_{\mu a}S_{j\nu}\langle\Phi_i^a|H|\Phi_j^j\rangle = 2S_{j\nu}(F_{\mu i} - \sum_k F_{ki}S_{\mu k}) \tag{A12}$$

and

$$S_{\mu i}S_{j\nu}\langle\Phi_i^i|H|\Phi_j^j\rangle = 2S_{\mu i}S_{j\nu}E_0 \tag{A13}$$

By collecting all terms, one gets the result quoted in eq 17 of the text. With similar steps, one also can derive the expression for $\langle\Phi_0|H|\Phi_i^\mu\rangle$ reported in eq 17.

AUTHOR INFORMATION

Corresponding Author

*E-mail: toffoli@units.it.

Notes

The authors declare no competing financial interest.

ACKNOWLEDGMENTS

This research has been partially supported by TUBITAK of Turkey (Grant No. 113F377) and CNR of Italy through a bilateral Italy−Turkey project. Computing resources used in this work were provided by CINECA (Bologna, Italy).

REFERENCES

(1) Hüfner, S. *Photoelectron Spectroscopy, Principles and Applications*, 3rd Edition; Springer−Verlag: Berlin, Heidelberg, New York, 2003; pp 1−662.
(2) Reinert, F.; Hüfner, S. *New J. Phys.* **2005**, *7*, 97.
(3) Carlson, T. A. *Photoelectron and Auger Spectroscopy*; Plenum Press: New York, 1975; pp 1−417.
(4) Feifel, R.; Piancastelli, M. *J. Electron Spectrosc. Relat. Phenom.* **2011**, *183*, 10−28.
(5) Wu, G.; Hockett, P.; Stolow, A. *Phys. Chem. Chem. Phys.* **2011**, *13*, 18447−18467.
(6) Becker, U.; Shirley, D. A. *Phys. Scr.* **1990**, *T31*, 56.
(7) Brage, T.; Fischer, C. F.; Miecznik, G. *J. Phys. B: At., Mol. Opt. Phys.* **1992**, *25*, 5289.
(8) Lucchese, R. R.; Takatsuka, K.; McKoy, V. *Phys. Rep.* **1986**, *131*, 147−221.
(9) Toffoli, D.; Lucchese, R. R.; Lebech, M.; Houver, J. C.; Dowek, D. *J. Chem. Phys.* **2007**, *126*, 054307.
(10) Toffoli, D.; Lucchese, R. R. *J. Chem. Phys.* **2004**, *120*, 6010−6018.
(11) Stratmann, R. E.; Lucchese, R. R. *J. Chem. Phys.* **1992**, *97*, 6384−6395.
(12) Stratmann, R. E.; Zurales, R. W.; Lucchese, R. R. *J. Chem. Phys.* **1996**, *104*, 8989−9000.
(13) McCurdy, C. W.; Rescigno, T. N. *Phys. Rev. A: At., Mol., Opt. Phys.* **1989**, *39*, 4487−4493.
(14) Schneider, B. I.; Rescigno, T. N. *Phys. Rev. A: At., Mol., Opt. Phys.* **1988**, *37*, 3749−3754.
(15) Rescigno, T. N.; McCurdy, C. W.; Orel, A. E.; Lengsfield, B. H. In *Computational Methods for Electron-Molecule Collisions*; Huo, W. M., Gianturco, F. A., Eds.; Springer: New York, 1995; Vol. *1*; pp 1−44.
(16) Yip, F. L.; McCurdy, C. W.; Rescigno, T. N. *Phys. Rev. A: At., Mol., Opt. Phys.* **2014**, *90*, 063421.
(17) Cacelli, I.; Carravetta, V.; Rizzo, A.; Moccia, R. *Phys. Rep.* **1991**, *205*, 283−351.
(18) Montuoro, R.; Moccia, R. *Chem. Phys.* **2003**, *293*, 281−308.
(19) Martín, F. *J. Phys. B: At., Mol. Opt. Phys.* **1999**, *32*, R197.
(20) Bachau, H.; Cormier, E.; Decleva, P.; Hansen, J. E.; Martín, F. *Rep. Prog. Phys.* **2001**, *64*, 1815.
(21) Marante, C.; González, J.; Corral, I.; Klinker, M.; Argenti, L.; Martín, F. *J. Phys.: Conf. Ser.* **2015**, *635*, 092013.
(22) Marante, C.; Argenti, L.; Martín, F. *Phys. Rev. A: At., Mol., Opt. Phys.* **2014**, *90*, 012506.
(23) Burke, P. G. *R-Matrix Theory of Atomic Collisions: Application to Atomic, Molecular and Optical Processes*; Springer: Berlin, 2011; pp 1−746.
(24) Tennyson, J. *Phys. Rep.* **2010**, *491*, 29−76.
(25) Stener, M.; Toffoli, D.; Fronzoni, G.; Decleva, P. *Theor. Chem. Acc.* **2007**, *117*, 943−956.
(26) Stener, M.; Fronzoni, G.; Decleva, P. *J. Chem. Phys.* **2005**, *122*, 234301.
(27) Toffoli, D.; Stener, M.; Fronzoni, G.; Decleva, P. *Chem. Phys.* **2002**, *276*, 25−43.

(28) Carr, J.; Galiatsatos, P.; Gorfinkiel, J.; Harvey, A.; Lysaght, M.; Madden, D.; Mašín, Z.; Plummer, M.; Tennyson, J.; Varambhia, H. *Eur. Phys. J. D* **2012**, *66*, 58.
(29) Harvey, A. G.; Brambila, D. S.; Morales, F.; Smirnova, O. *J. Phys. B: At., Mol. Opt. Phys.* **2014**, *47*, 215005.
(30) Brambila, D. S.; Harvey, A. G.; Mašín, Z.; Gorfinkiel, J. D.; Smirnova, O. *J. Phys. B: At., Mol. Opt. Phys.* **2015**, *48*, 245101.
(31) Brigg, W. J.; Harvey, A. G.; Dzarasova, A.; Mohr, S.; Brambila, D. S.; Morales, F.; Smirnova, O.; Tennyson, J. *Jpn. J. Appl. Phys.* **2015**, *54*, 06GA02.
(32) Majety, V. P.; Zielinski, A.; Scrinzi, A. *New J. Phys.* **2015**, *17*, 063002.
(33) Majety, V. P.; Scrinzi, A. *Phys. Rev. Lett.* **2015**, *115*, 103002.
(34) Majety, V. P.; Scrinzi, A. *J. Phys. B: At., Mol. Opt. Phys.* **2015**, *48*, 245603.
(35) Gozem, S.; Gunina, A. O.; Ichino, T.; Osborn, D. L.; Stanton, J. F.; Krylov, A. I. *J. Phys. Chem. Lett.* **2015**, *6*, 4532−4540.
(36) Ponzi, A.; Angeli, C.; Cimiraglia, R.; Coriani, S.; Decleva, P. *J. Chem. Phys.* **2014**, *140*, 204304.
(37) Ruberti, M.; Yun, R.; Gokhberg, K.; Kopelke, S.; Cederbaum, L. S.; Tarantelli, F.; Averbukh, V. *J. Chem. Phys.* **2013**, *139*, 144107.
(38) Cukras, J.; Coriani, S.; Decleva, P.; Christiansen, O.; Norman, P. *J. Chem. Phys.* **2013**, *139*, 094103.
(39) Nesbet, R. K. *Variational Methods in Electron-Atom Scattering Theory*; Plenum Press: New York, 1980; pp 1−228.
(40) Decleva, P.; Lisini, A.; Venuti, M. *J. Phys. B: At., Mol. Opt. Phys.* **1994**, *27*, 4867.
(41) Venuti, M.; Decleva, P. *J. Phys. B: At., Mol. Opt. Phys.* **1997**, *30*, 4839.
(42) Foresman, J. B.; Head-Gordon, M.; Pople, J. A.; Frisch, M. J. *J. Phys. Chem.* **1992**, *96*, 135−149.
(43) Qiu, Y.; Fischer, C. F. *J. Comput. Phys.* **1999**, *156*, 257−271.
(44) Krause, P.; Klamroth, T.; Saalfrank, P. *J. Chem. Phys.* **2005**, *123*, 074105.
(45) Krause, P.; Schlegel, H. B. *J. Phys. Chem. A* **2015**, *119*, 10212−10220.
(46) Krause, P.; Schlegel, H. B. *J. Phys. Chem. Lett.* **2015**, *6*, 2140−2146.
(47) Sonk, J. A.; Schlegel, H. B. *J. Phys. Chem. A* **2012**, *116*, 7161−7168.
(48) Greenman, L.; Ho, P. J.; Pabst, S.; Kamarchik, E.; Mazziotti, D. A.; Santra, R. *Phys. Rev. A: At., Mol., Opt. Phys.* **2010**, *82*, 023406.
(49) Karamatskou, A.; Pabst, S.; Chen, Y.-J.; Santra, R. *Phys. Rev. A: At., Mol., Opt. Phys.* **2014**, *89*, 033415.
(50) Goetz, R. E.; Karamatskou, A.; Santra, R.; Koch, C. P. *Phys. Rev. A: At., Mol., Opt. Phys.* **2016**, *93*, 013413.
(51) Hochstuhl, D.; Bonitz, M. *Phys. Rev. A: At., Mol., Opt. Phys.* **2012**, *86*, 053424.
(52) Pabst, S.; Greenman, L.; Mazziotti, D. A.; Santra, R. *Phys. Rev. A: At., Mol., Opt. Phys.* **2012**, *85*, 023411.
(53) Pabst, S.; Greenman, L.; Ho, P. J.; Mazziotti, D. A.; Santra, R. *Phys. Rev. Lett.* **2011**, *106*, 053003.
(54) Altmann, S. L.; Cracknell, A. P. *Rev. Mod. Phys.* **1965**, *37*, 19−32.
(55) Starace, A. F. In *Handbuch der Physik*; Mehlhorn, W., Ed.; Springer−Verlag: Berlin, 1982; Vol. *31*; pp 1−121.
(56) Chandra, N. *Chem. Phys.* **1986**, *108*, 301−315.
(57) Chandra, N. *J. Phys. B: At. Mol. Phys.* **1987**, *20*, 3405.
(58) Szabo, A.; Ostlund, N. S. *Modern Quantum Chemistry, Introduction to Advanced Electronic Structure Theory*; McGraw−Hill: New York, 1989; pp 1−480.
(59) Werner, H.-J.; Knowles, P. J.; Knizia, G.; Manby, F. R.; Schütz, M. *WIREs Comput. Mol. Sci.* **2012**, *2*, 242−253.
(60) W. Gropp, E. L.; Skjellum, A. *Portable Parallel Programming with the Message-Passing Interface*; Using MPI, Third Edition; MIT Press: Cambridge, MA, 2014; pp 1−350.
(61) Grimm, F. A. *Chem. Phys.* **1983**, *81*, 315−327.
(62) Ibuki, T.; Cooper, G.; Brion, C. *Chem. Phys.* **1989**, *129*, 295−309.
(63) Brennan, J. G.; Cooper, G.; Green, J. C.; Payne, M. P.; Redfern, C. M. *J. Electron Spectrosc. Relat. Phenom.* **1987**, *43*, 297−305.
(64) Mehaffy, D.; Keller, P. R.; Taylor, J. W.; Carlson, T. A.; Krause, M. O.; Grimm, F. A.; Allen, J. D. *J. Electron Spectrosc. Relat. Phenom.* **1982**, *26*, 213−221.
(65) Grimm, F.; Whitley, T.; Keller, P.; Taylor, J. *Chem. Phys.* **1991**, *154*, 303−309.
(66) Brescansin, L.; Lee, M.-T.; Machado, L.; Lima, M.; McKoy, V. *Braz. J. Phys.* **1997**, *27*, 468−474.
(67) van Leeuwen, R.; Baerends, E. J. *Phys. Rev. A: At., Mol., Opt. Phys.* **1994**, *49*, 2421−2431.
(68) Samson, J. A. R.; He, Z. X.; Yin, L.; Haddad, G. N. *J. Phys. B: At., Mol. Opt. Phys.* **1994**, *27*, 887.
(69) Chan, W. F.; Cooper, G.; Brion, C. E. *Phys. Rev. A: At., Mol., Opt. Phys.* **1991**, *44*, 186−204.
(70) Chan, W. F.; Cooper, G.; Guo, X.; Brion, C. E. *Phys. Rev. A: At., Mol., Opt. Phys.* **1992**, *45*, 1420−1433.
(71) Samson, J.; Stolte, W. *J. Electron Spectrosc. Relat. Phenom.* **2002**, *123*, 265−276.
(72) Dehmer, J. *J. Phys., Colloq.* **1978**, *39*, C4-42−C4-50.
(73) Schartner, K. H.; Magel, B.; Mobus, B.; Schmoranzer, H.; Wildberger, M. *J. Phys. B: At., Mol. Opt. Phys.* **1990**, *23*, L527.
(74) Dreuw, A.; Head-Gordon, M. *Chem. Rev.* **2005**, *105*, 4009−4037.
(75) Chan, W. F.; Cooper, G.; Guo, X.; Burton, G. R.; Brion, C. E. *Phys. Rev. A: At., Mol., Opt. Phys.* **1992**, *46*, 149−171.
(76) Houlgate, R.; West, J.; Codling, K.; Marr, G. *J. Electron Spectrosc. Relat. Phenom.* **1976**, *9*, 205−209.
(77) Möbus, B.; Magel, B.; Schartner, K.-H.; Langer, B.; Becker, U.; Wildberger, M.; Schmoranzer, H. *Phys. Rev. A: At., Mol., Opt. Phys.* **1993**, *47*, 3888−3893.
(78) Samson, J. A. R.; Haddad, G. N. *J. Opt. Soc. Am. B* **1994**, *11*, 277−279.
(79) Zimmermann, B.; McKoy, V.; Southworth, S. H.; Kanter, E. P.; Krässig, B.; Wehlitz, R. *Phys. Rev. A: At., Mol., Opt. Phys.* **2015**, *91*, 053410.
(80) Sánchez, I.; Martín, F. *J. Phys. B: At., Mol. Opt. Phys.* **1997**, *30*, 679.
(81) Chan, W.; Cooper, G.; Brion, C. *Chem. Phys.* **1993**, *178*, 387−400.
(82) Banna, M. S.; McQuaide, B. H.; Malutzki, R.; Schmidt, V. *J. Chem. Phys.* **1986**, *84*, 4739−4744.
(83) Tan, K.; Brion, C.; Van der Leeuw, P.; van der Wiel, M. *Chem. Phys.* **1978**, *29*, 299−309.
(84) Truesdale, C. M.; Southworth, S.; Kobrin, P. H.; Lindle, D. W.; Thornton, G.; Shirley, D. A. *J. Chem. Phys.* **1982**, *76*, 860−865.
(85) Ruberti, M.; Averbukh, V.; Decleva, P. *J. Chem. Phys.* **2014**, *141*, 164126.
(86) Toffoli, D.; Decleva, P. *J. Chem. Phys.* **2012**, *137*, 134103.
(87) Sturm, E. J.; Mazziotti, D. A. *Mol. Phys.* **2016**, *114*, 335−343.
(88) Stratmann, R. E.; Lucchese, R. R. *J. Chem. Phys.* **1995**, *102*, 8493−8505.
(89) Botting, S. K.; Lucchese, R. R. *Phys. Rev. A: At., Mol., Opt. Phys.* **1997**, *56*, 3666−3674.
(90) Lin, P.; Lucchese, R. R. *J. Chem. Phys.* **2002**, *117*, 4348−4360.
(91) Hochstuhl, D.; Hinz, C.; Bonitz, M. *Eur. Phys. J.: Spec. Top.* **2014**, *223*, 177−336.
(92) Rescigno, T. N.; Lengsfield, B. H.; Orel, A. E. *J. Chem. Phys.* **1993**, *99*, 5097−5103.
(93) Lengsfield, B. H.; Rescigno, T. N. *Phys. Rev. A: At., Mol., Opt. Phys.* **1991**, *44*, 2913−2920.